PHOTONICS Research

High-order mode lasing in all-FMF laser cavities

Teng Wang, Ao Yang, Fan Shi, Yiping Huang, Jianxiang Wen, and Xianglong Zeng*

Key Laboratory of Specialty Fiber Optics and Optical Access Networks, Joint International Research Laboratory of Specialty Fiber Optics and Advanced Communication, Shanghai Institute for Advanced Communication and Data Science, Shanghai University, Shanghai 200444, China
**Corresponding author: zenglong@shu.edu.cn*

Received 20 September 2018; revised 1 November 2018; accepted 12 November 2018; posted 13 November 2018 (Doc. ID 346426); published 13 December 2018

We experimentally demonstrate two kinds of all few-mode fiber (FMF) ring lasers with high-order mode (HOM) oscillation in the laser cavity. One kind is a switchable-wavelength all-FMF HOM laser with an output of tunable optical vortex beams (OVBs); the other is a *Q*-switched all-FMF HOM laser with an output of pulsed cylindrical vector beams (CVBs). The lasers are composed of all-FMF components and few-mode erbium-doped fiber. A Sagnac interferometer made of a 3 dB FMF coupler functions as the wavelength selector, and switchable multiwavelength tunable OVBs are experimentally realized. Carbon nanotube-based saturable absorbers and the nonlinear polarization rotation technique are used to achieve *Q*-switched CVB lasers. This is the first report, to our knowledge, on the generation of switchable-wavelength and *Q*-switched HOM beams in all-FMF laser cavities.

https://doi.org/10.1364/PRJ.7.000042

1. INTRODUCTION

Mode-division multiplexing (MDM) and wavelength-division multiplexing (WDM) have been advancing rapidly for several years, to increase the data-carrying capacity of a single few-mode fiber (FMF) [1–6]. High-order mode (HOM) lasers and multiwavelength fiber lasers have attracted much attention due to their potential applications in MDM and WDM. On the other hand, HOMs also have unique spatial intensity and polarization distribution properties, such as cylindrical vector beams (CVBs) and optical vortex beams (OVBs) [7–10]. There have been many attempts to generate and manipulate HOM beams based on fiber lasers. Continuous-wave (CW), pulsed, narrow-linewidth, and multiwavelength HOM beams have been obtained using mode-selective couplers (MSCs) [11–16], few-mode fiber gratings [17–22], a lateral offset splicing technique [23], and so on. Multiwavelength HOM lasers are considered to be especially excellent sources for optical coherent communication and sensing systems; these have developed rapidly in recent years [24–26]. However, all research about HOMs to date is based on single-mode fiber (SMF) lasers and mode converters, and the efficiency and mode quality are greatly limited by the mode-conversion efficiency and bandwidth.

Few-mode fiber lasers provide a new way to directly generate HOM beams with high efficiency and modal purity; they also open up new directions in researching nonlinear wave propagation, high-power fiber lasers, and random lasers [27–31]. Compared with conventional SMF lasers, transverse mode control is a very novel and important issue in FMF laser cavities. Optical vortices with tunable orbital angular momentum (OAM) can carry more information due to the utilization of polarization [32,33]. Tunable OVBs generated in switchable multiwavelength all-FMF lasers have the advantages of high efficiency, high modal purity, wavelength flexibility, and high coherence. Thus, they are more appropriate for applications in co-multiplexed systems. *Q*-switched mode locking (QML) is an operation regime of mode-locked lasers with strong fluctuation of the pulse energy [34]. Nevertheless, the passive HOM *Q*-switching in an all-FMF laser cavity has not been investigated so far. Saturable absorber (SA) and nonlinear polarization rotation (NPR) techniques are effective methods of achieving a compact HOM pulse, and have been widely used in ultrafast fiber lasers. Due to the high peak power and annular intensity distribution, HOM pulses can be used in many applications, such as materials processing [35].

In this paper, we propose novel and compact all-FMF lasers with outputs of switchable wavelength tunable OVBs and pulsed CVBs. The OVB tunability in the fiber laser is experimentally realized by adjusting a polarizer at the output end of the FMF. This is the first report, to our knowledge, on the generation of switchable-wavelength OVBs and pulsed CVBs based on all-FMF lasers. Switchable multiwavelength OVBs with tunable OAM are desirable for multiplexing, exchanging, and routing to further improve the capacity of optical fiber transmission.

2. MULTIWAVELENGTH FEW-MODE FIBER LASER

The experimental setup of a switchable multiwavelength FMF (four-mode step-index fiber, $D_{core} = 18.5$ μm) laser based on

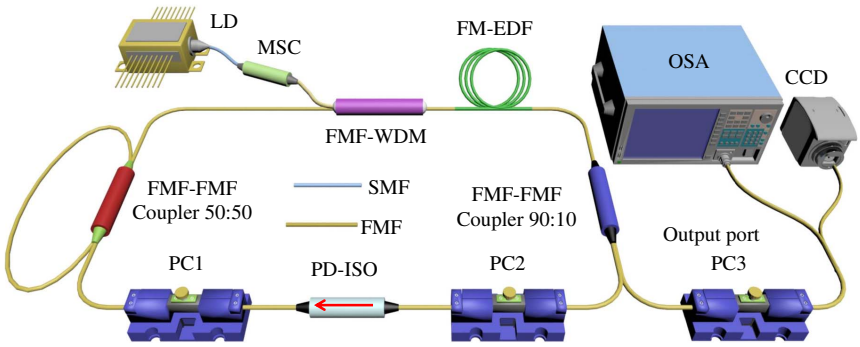

Fig. 1. Schematic of a multiwavelength all-FMF ring laser. LD, laser diode; MSC, mode-selective coupler; FMF-WDM, few-mode fiber wavelength division multiplexer; FM-EDF, few mode erbium-doped fiber; PD-ISO, polarization dependent isolator; PC, polarization controller; OSA, optical spectrum analyzer; CCD, charge-coupled device, infrared camera.

a Sagnac interferometer is shown in Fig. 1. Here, we use a ring refractive index distribution few-mode erbium-doped fiber (FM-EDF, $D_{\text{core}} = 6$ μm, $D_{\text{ring}} = 17.5$ μm) as the gain medium [36]. A 980 nm MSC is used to achieve the pump mode conversion from LP_{01} mode to LP_{11} mode. HOM pump light is injected into the FM-EDF through an FMF wavelength division multiplexer, which works as a wavelength multiplexer between LP_{11} modes at 980/1550 nm. Identical LP_{11} modes of pump and signal are crucial to obtain efficient HOM gain and inhibit the fundamental mode oscillation in the FM-EDF. An all-FMF isolator is inserted into the cavity to force the unidirectional operation of the laser. An FMF–FMF coupler with a power-splitting ratio of 90:10 is used to extract the LP_{11} mode power out of the FMF cavity. The length of the FM-EDF is 1.9 m, and the total cavity length is 8.6 m. The output spectra are analyzed by an optical spectrum analyzer (OSA, Yokogawa, AQ6370C). The near-field intensity distributions of output signals are recorded by a CCD camera (InGaAs camera, model C10633-23, from Hamamatsu Photonics).

High-order LP_{11} mode amplification in an all-FMF laser has been extensively investigated in our previous paper [28]. It is clear that both the pump and signal mode can be kept very well in the FM-EDF and is mainly LP_{11} mode. Transverse-mode competition can also be controlled by designing new types of FMF and gain fiber, such as ring refractive index profile fiber that would suppress the fundamental mode. Two polarization controllers (PCs) and a polarization dependent isolator are used to control the evolution of mode polarization inside the laser cavity, in which the NPR effect induces intensity-dependent loss (IDL). The IDL is different for individual wavelengths, which can be used to alleviate the mode competition and also to choose the oscillation mode.

The broadband Sagnac interferometer is made of a 3 dB FMF–FMF coupler. The ring length of the Sagnac loop is approximately 1 m. The typical transmission of the Sagnac interferometer with the periodic wavelength response covers the whole C-band. The transmission spectra of the LP_{01} and LP_{11} modes are shown in Figs. 2(a) and 2(b), respectively. Figures 2(c) and 2(d) show the transmission spectra from 1540 to 1550 nm. The interference spectrum is caused by a phase difference between two beams, which are in the same path but in opposite directions. At a certain wavelength, output power reaches the maximum (minimum) when the phase difference equals the odd (even) times of π. In the laser cavity, this special comb filter acts as the wavelength selector. The peak-to-notch contrast ratio of the Sagnac interferometer is around 12 dB. Here, the peak spacings are 2.5 and 2.6 nm, respectively, which are determined by the perimeter of the Sagnac loop and the effective refractive index of the incident mode. The unsmoothness of the transmission spectrum in Fig. 2(b) is due to the impurity of the LP_{11} mode broadband light source.

The fiber laser can be easily tuned to operate in the single-wavelength LP_{11} mode oscillation state under the pump power of 300 mW. By adjusting the PCs, switchable single wavelength output is observed. Lasing wavelengths can be both individually switched and widely tuned among 13 channels, from 1562 to 1593.2 nm with 2.6 nm spacing, which are dependent on the gain spectra and the saturated signal level of the FM-EDF. As shown in Fig. 3(a), the oscillation wavelengths correspond to the transmission spectra of the Sagnac interferometer employed as 1562.0, 1564.6, 1567.2, 1569.8, and 1572.4 nm, respectively. The 3 dB bandwidth of the generated single-wavelength LP_{11} mode beam is 0.12 nm. The central wavelength remains unchanged when increasing the pump power. The signal-to-noise ratios (SNRs) of all channel outputs are nearly 36 dB, and the fluctuation is less than 0.1 dB.

By increasing the pump power to 400 mW and adjusting the PCs appropriately, the multiwavelength state occurs. Adjacent dual-wavelength is successively tuned out in the lasing channels. Output spectra of stable adjacent double-, triple-, and quadruple-wavelength lasing operations are shown in Figs. 3(b)–3(d), respectively. The output dual wavelengths are located at 1564.6 and 1567.2 nm, with a spacing of 2.6 nm. The triple and quadruple wavelengths are with the same spacing. The stable multiwavelength laser output is dependent on the cavity loss induced by the NPR effect. The SNRs of all channels are over 35 dB, indicating the high stability of the laser output. The output triple-wavelength spectra are repeatedly scanned every 2 min, as shown in Fig. 4(a). The fluctuation of output power is less than 1.5 dB, and central wavelengths of different channels are maintained within 0.02 nm in 10 min, which shows the stability of the output laser, as shown in Fig. 4(b).

The intensity distributions from the output port are monitored with a CCD camera. The output beams before PC3 are

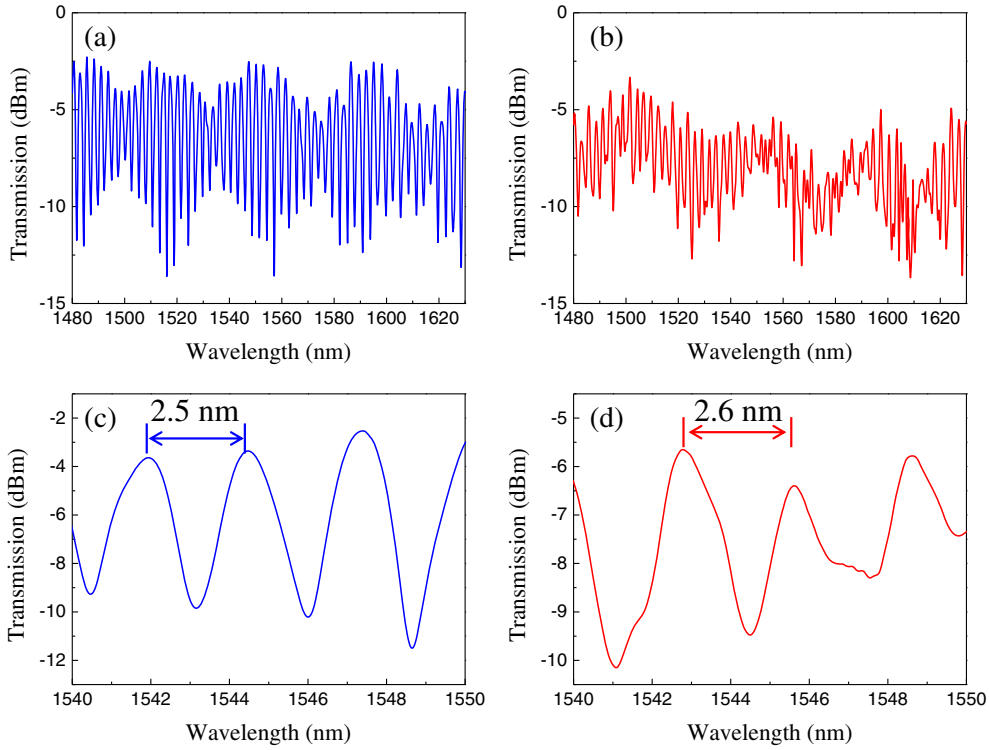

Fig. 2. Spectral response of an all-FMF Sagnac interferometer. Transmission spectra with different launch modes: (a) LP_{01} mode and (b) LP_{11} mode. (c) and (d) Transmission spectra from 1540 to 1550 nm.

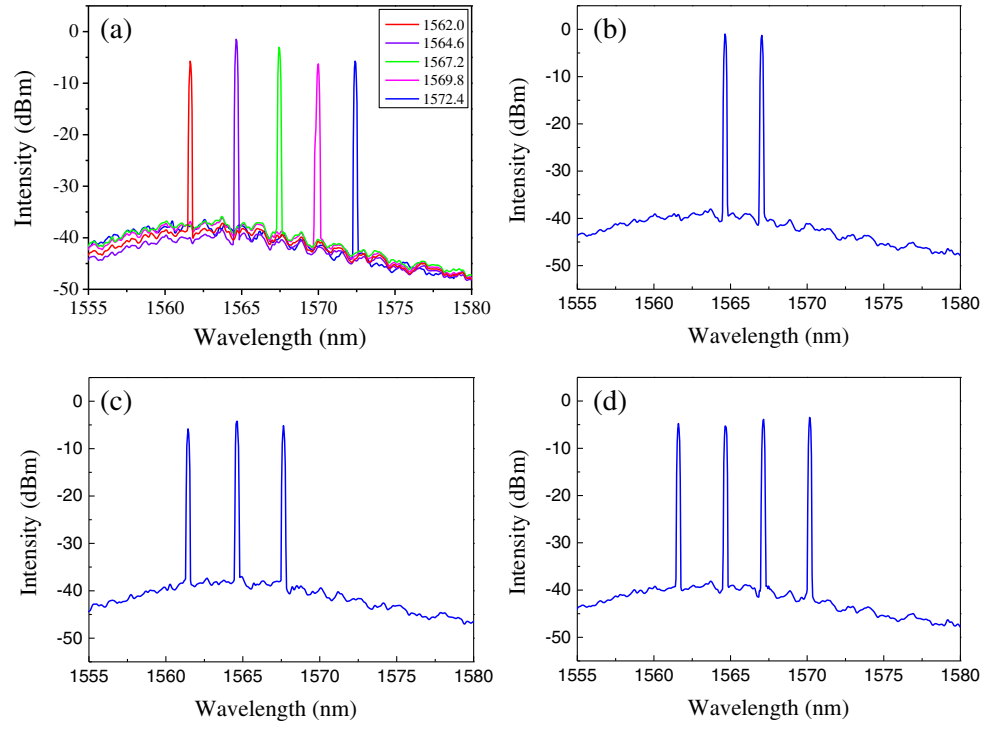

Fig. 3. Spectra of multiwavelength operations when adjusting the PCs. Output spectra of successively tunable (a) single-, (b) dual-, (c) triple-, and (d) quadruple-wavelength lasing operations.

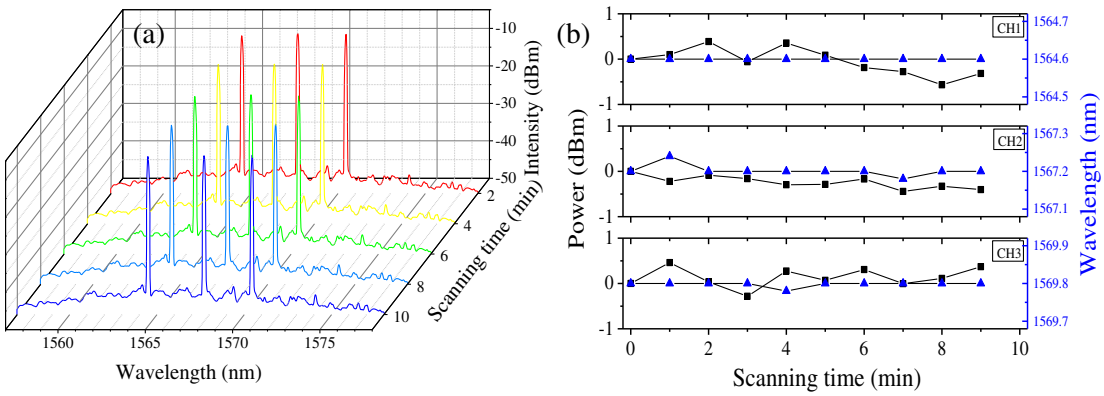

Fig. 4. Stability of triple-wavelength output spectra. (a) Repeated scans of the triple-wavelength output spectrum every two minutes. (b) Power fluctuation (black) and central wavelength (blue) of each channel.

mixed $LP_{11a/b}$ modes, as shown in Figs. 5(a) and 5(e). $LP_{11a/b}$ modes are degenerated by four vector modes (TM_{01}, HE_{21}^{even}, HE_{21}^{odd}, TE_{01}) which have similar propagation constants. Tunable OVBs with different topological charges can be produced by combining different vector modes HE_{21}^{even} (HE_{21}^{odd}) and TE_{01} (TM_{01}) with a $\pi/2$ phase shift. By adjusting the rotating angle and pressure of PC3, a $\pi/2$ phase shift between two vector modes is achieved [7,37]. As shown in Figs. 5(b) and 5(f), the outputs are tunable OVBs with annular intensity profiles and two opposite helical phase fronts in two orthogonal polarizations.

To testify the topological charge of the output beams in different polarization directions, a polarizer is added between the FMF output port and CCD camera. Donut-shaped and two-lobe-shaped intensity patterns are observed alternately by rotating the polarization direction of the polarizer, which is marked with double-headed arrows indicating the transmission direction. Figures 5(d1), 5(d3), 5(h1), and 5(h3) show the interference patterns of the donut-shaped beams with a reference Gaussian beam (mode conversion from OAM mode to LP_{01} mode), which indicates that donut-shaped beams are vortex beams with a topological charge of 1. The clockwise and counter-clockwise spiral interference patterns indicate OAM_{-1} mode and OAM_{+1} mode, respectively, which show that tunable OVBs are successfully achieved at the output FMF port. The purity of tunable OVBs is verified by using

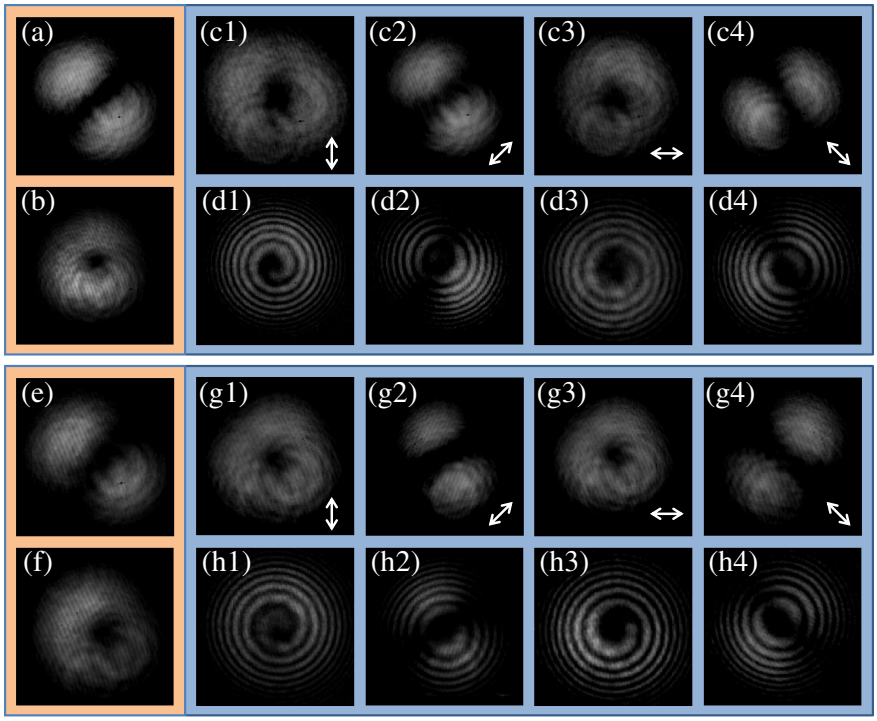

Fig. 5. Near-field intensity distributions of the FMF laser. (a) Single-wavelength LP_{11} mode and (b) corresponding tunable OVBs when pressing the end of the FMF. (e) Triple-wavelength LP_{11} mode and (f) corresponding tunable OVBs. (c1)–(c4) and (g1)–(g4) Near-field intensity patterns with rotation of a polarizer. (d1)–(d4) and (h1)–(h4) Corresponding interference patterns. The white arrows indicate the polarization orientation.

the tight bend approach [38] and estimated to be in excess of 96%.

3. Q-SWITCHED FEW-MODE FIBER LASER

The experimental setup of the Q-switched LP_{11} mode all-FMF ring cavity fiber laser is shown in Fig. 6. Carbon nanotube (CNT) dispersed in polyvinyl alcohol (PVA) film sandwiched between two optical connectors is used as an SA. The modulation depth of the CNT-based SA is 9.7%. Both the CNT-SA and the NPR technique are applied to achieve self-started QML operation in the FMF laser. The principle of NPR is based on the rotation of the polarization ellipse resulting from the optical Kerr nonlinearity [39]. Due to the current laser cavity configuration and high welding losses between FM-EDF and FMF, self-started QML initiation via NPR is difficult. A CNT-SA can independently initiate QML. However, NPR, as an additional pulse-formation mechanism, ensures the laser generation stabilization [40]. The output signal is recorded by an OSA, a CCD camera, and the time-domain waveform is analyzed by an oscilloscope (Tektronix, MSO4104).

Once the pump power increases to 180 mW, the self-started Q-switching state occurs. Q-switched outputs at a pump power of 400 mW are shown in Fig. 7. The output central wavelength is 1595.98 nm, with a 3 dB bandwidth of 0.1 nm, as shown in Fig. 7(a). Figure 7(b) shows the Q-switched pulse train, which has a repetition rate of 10.6 kHz, corresponding to a time interval of 137 μs. From the profile of the single pulse in Fig. 7(c), we can see that the output pulses have a full width at half-maximum of 21 μs, with an asymmetric temporal

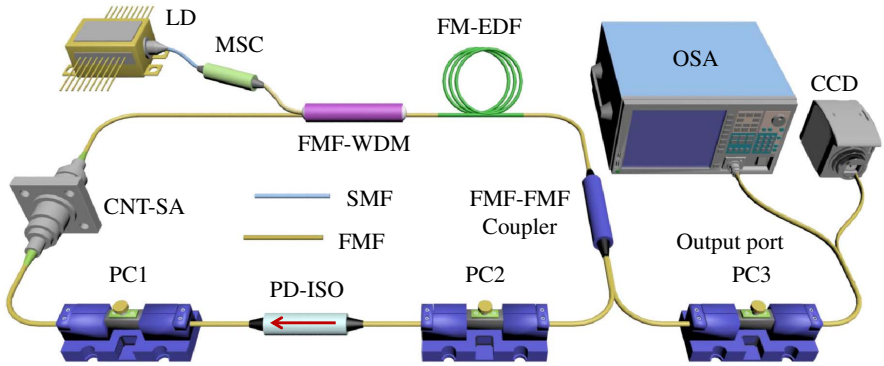

Fig. 6. Schematic of Q-switched all-FMF ring laser. CNT-SA, carbon nanotube saturable absorber.

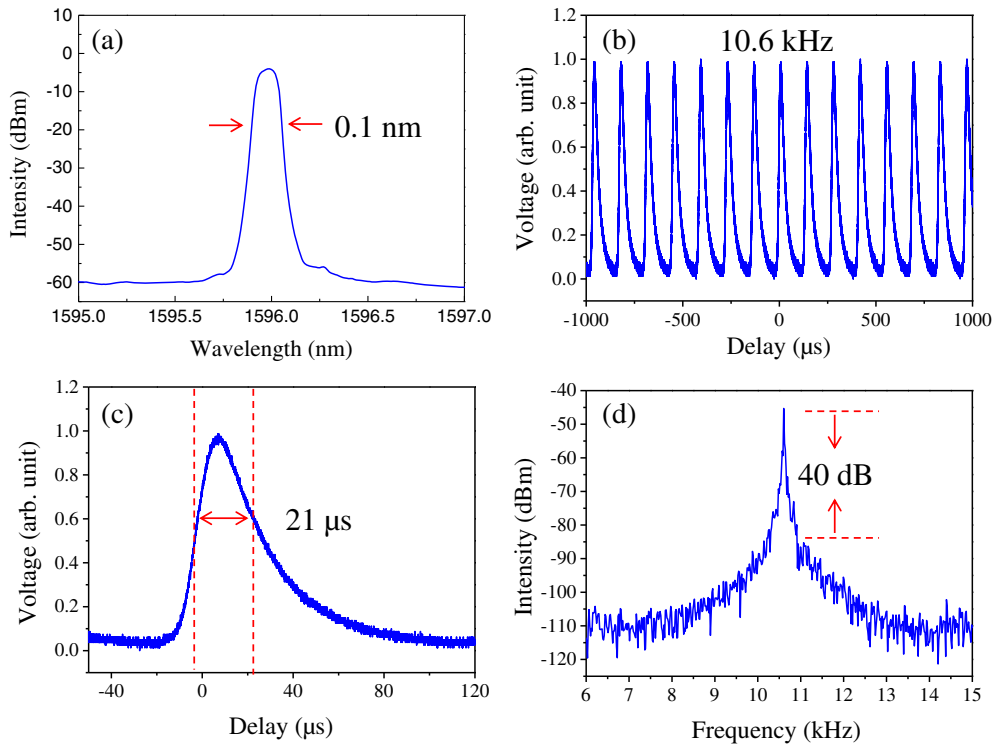

Fig. 7. (a) Output optical spectrum of a Q-switched fiber laser. (b) Typical Q-switched pulse train. (c) Single pulse envelope. (d) RF spectrum.

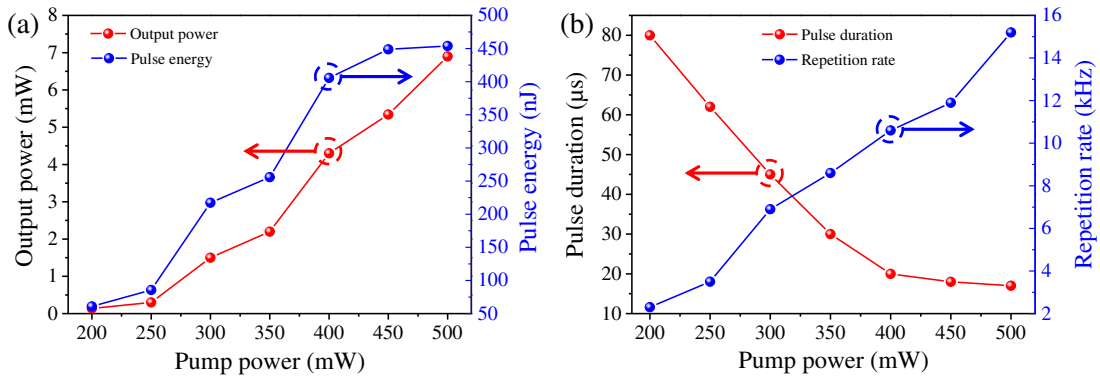

Fig. 8. (a) Average output power and pulse energy versus pump power. (b) Pulse duration and repetition rate versus pump power.

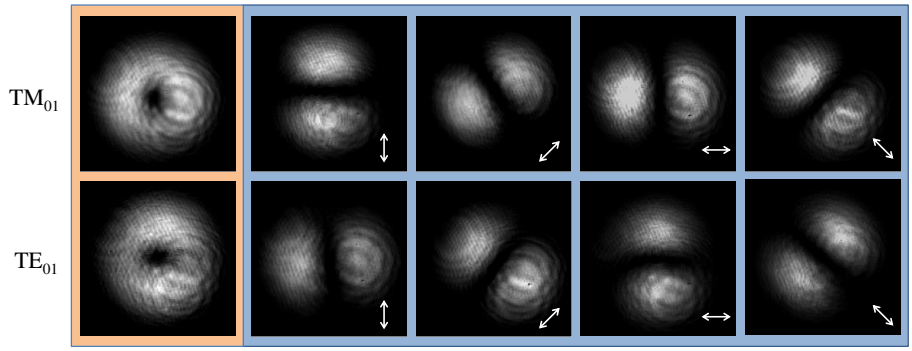

Fig. 9. Near-field intensity distribution of TM_{01} (top) and TE_{01} (bottom) modes with rotation of a polarizer.

profile. Also, we have measured the corresponding radio frequency (RF) spectrum, with a resolution bandwidth of 10 Hz. As shown in Fig. 7(d), the central frequency is 10.6 kHz, which agrees with the pulse repetition rate very well. The SNR is over 40 dB, indicating the high stability of the laser output.

Figure 8 shows the evolution of the *Q*-switched pulse performance as the pump power increases from 200 to 500 mW. As shown in Fig. 8(a), the average output power and the pulse energy increase with the pump power. Once the pump power exceeds 500 mW, the *Q*-switched operation becomes unstable and changes to CW operation, but it can be recovered by decreasing the pump power again. Figure 8(b) shows the evolution of the repetition rate and pulse width versus pump power. When the repetition rate of the *Q*-switched pulses increases from 2.3 to 15.2 kHz, the pulse duration decreases from 80 to 18 μs consistently.

CVBs with different polarization states can also be excited. PC3 is used as a rotator and a flat slab to press and rotate the FMF, which changes the symmetric fiber structure and mode propagation constants. By adjusting PC3, all the vector modes can be converted to a specific vector mode through efficient mode coupling [11,41]. The radially polarized beam (RPB) is TM_{01} mode and the azimuthally polarized beam (APB) is TE_{01} mode. Figure 9 shows the spatial distribution of the output beams, which have annular intensity profiles with a dark spot at the center. After passing through a polarizer, the donut-shaped mode patterns are filtered into two parts that rotate with the polarizer, which are the typical characteristic of CVBs. The dark bands of the RPB/APB are perpendicular/parallel to the transmission axis of the polarizer. The near-field images present uniform $TM_{0,1}$ and $TE_{0,1}$ mode distributions, confirming that *Q*-switched radially and azimuthally polarized output beams with high purity are achieved. The radial/azimuthal polarization purity can be quantified by the vector mode decomposition technique [42].

4. CONCLUSION

In conclusion, we have proposed and experimentally demonstrated a new method of generating tunable OVBs in a switchable-wavelength all-FMF laser, based on a Sagnac interferometer, for the first time to our knowledge. The laser can realize stable single-, dual-, triple-, and quadruple-wavelength outputs. The OVB tunability in the fiber laser is experimentally realized by adjusting a polarizer at the output end of the FMF. The OAM of OVBs has a topological charge that could be continuously varied between −1 and +1. Pulsed CVBs are also obtained in a *Q*-switched all-FMF laser based on CNT-SA and NPR. This work is promising for efficiently obtaining HOM beams in FMF lasers. More efficient generation of HOM beams is anticipated to be implemented by optimizing the losses of the fiber cavity. These laser sources can find applications in co-multiplexed systems and materials processing.

Funding. National Natural Science Foundation of China (NSFC) (61635006, 91750108, 61520106014); Science and Technology Commission of Shanghai Municipality (STCSM) (16520720900).

Acknowledgment. Xianglong Zeng acknowledges the Program for Professor of Special Appointment (Eastern Scholar) at Shanghai Institutions of Higher Learning.

REFERENCES

1. D. J. Richardson, J. M. Fini, and L. E. Nelson, "Space-division multiplexing in optical fibres," Nat. Photonics **7**, 354–362 (2013).
2. H. Chen, C. Jin, B. Huang, N. Fontaine, R. Ryf, K. Shang, N. Grégoire, S. Morency, R. J. Essiambre, and G. Li, "Integrated cladding-pumped multicore few-mode erbium-doped fibre amplifier for space-division-multiplexed communications," Nat. Photonics **10**, 529–533 (2016).
3. J. V. Weerdenburg, R. Ryf, J. C. Alvarado-Zacarias, R. A. Alvarez-Aguirre, N. K. Fontaine, H. Chen, R. A. Correa, Y. Sun, L. Gruner-Nielsen, and R. Jensen, "138 Tbit/s mode- and wavelength multiplexed transmission over 6-mode graded-index fiber," J. Lightwave Technol. **36**, 1369–1374 (2018).
4. T. Feng, D. Ding, F. Yan, Z. Zhao, H. Su, and X. S. Yao, "Widely tunable single-/dual-wavelength fiber lasers with ultra-narrow linewidth and high OSNR using high quality passive subring cavity and novel tuning method," Opt. Express **24**, 19760–19768 (2016).
5. Q. Zhang, X. Zeng, F. Pang, M. Wang, and T. Wang, "Switchable multiwavelength fiber laser by using a compact in-fiber Mach-Zehnder interferometer," J. Opt. **14**, 045403 (2012).
6. X. Liu, L. Zhan, S. Luo, Y. Wang, and Q. Shen, "Individually switchable and widely tunable multiwavelength erbium-doped fiber laser based on cascaded mismatching long-period fiber gratings," J. Lightwave Technol. **29**, 3319–3326 (2011).
7. T. Wang, F. Wang, F. Shi, F. Pang, S. Huang, T. Wang, and X. Zeng, "Generation of femtosecond optical vortex beams in all-fiber mode-locked fiber laser using mode selective coupler," J. Lightwave Technol. **35**, 2161–2166 (2017).
8. K. Wei, W. Zhang, L. Huang, D. Mao, F. Gao, T. Mei, and J. Zhao, "Generation of cylindrical vector beams and optical vortex by two acoustically induced fiber gratings with orthogonal vibration directions," Opt. Express **25**, 2733–2741 (2017).
9. W. Zhang, L. Huang, K. Wei, P. Li, B. Jiang, D. Mao, F. Gao, T. Mei, G. Zhang, and J. Zhao, "High-order optical vortex generation in a few-mode fiber via cascaded acoustically driven vector mode conversion," Opt. Lett. **41**, 5082–5085 (2016).
10. J. Wang, "Advances in communications using optical vortices," Photon. Res. **4**, B14–B28 (2016).
11. F. Wang, F. Shi, T. Wang, F. Pang, T. Wang, and X. Zeng, "Method of generating femtosecond cylindrical vector beams using broadband mode converter," IEEE Photon. Technol. Lett. **29**, 747–750 (2017).
12. Y. Shen, G. Ren, Y. Yang, S. Yao, Y. Wu, Y. Jiang, Y. Xu, W. Jin, B. Zhu, and S. Jian, "Switchable narrow linewidth fiber laser with LP_{11} transverse mode output," Opt. Laser Technol. **98**, 1–6 (2018).
13. T. Wang, F. Wang, F. Shi, F. Pang, S. Huang, T. Wang, and X. Zeng, "All-fiber mode-locked vortex laser with a broadband mode coupler," in *Optical Fiber Communications Conference and Exhibition (OFC)* (Optical Society of America, 2017), paper Tu3J.2.
14. D. Mao, Z. He, H. Lu, M. Li, W. Zhang, X. Cui, B. Jiang, and J. Zhao, "All-fiber radially/azimuthally polarized lasers based on mode coupling of tapered fibers," Opt. Lett. **43**, 1590–1593 (2018).
15. Y. Huang, F. Shi, T. Wang, X. Liu, X. Zeng, F. Pang, T. Wang, and P. Zhou, "High-order mode Yb-doped fiber lasers based on mode-selective couplers," Opt. Express **26**, 19171–19181 (2018).
16. H. Wan, J. Wang, Z. Zhang, J. Wang, S. Ruan, and L. Zhang, "Passively mode-locked ytterbium-doped fiber laser with cylindrical vector beam generation based on mode selective coupler," J. Lightwave Technol. **36**, 3403–3407 (2018).
17. Y. Zhao, T. Wang, C. Mou, Z. Yan, Y. Liu, and T. Wang, "All-fiber vortex laser generated with few-mode long-period gratings," IEEE Photon. Technol. Lett. **30**, 752–755 (2018).
18. Y. Zhou, K. Yan, R. S. Chen, C. Gu, L. X. Xu, A. T. Wang, and Q. Zhan, "Resonance efficiency enhancement for cylindrical vector fiber laser with optically induced long period grating," Appl. Phys. Lett. **110**, 161104 (2017).
19. A. Wang, B. Sun, C. Gu, D. Chung, G. Chen, L. Xu, and Q. Zhan, "Mode-locked all-fiber laser producing radially polarized rectangular pulses," Opt. Lett. **40**, 1691–1694 (2015).
20. X. Zhang, W. Zhang, C. Li, D. Mao, F. Gao, L. Huang, D. Yang, T. Mei, and J. Zhao, "All-fiber cylindrical vector beams laser based on an acoustically-induced fiber grating," J. Opt. **20**, 075608 (2018).
21. R. Chen, F. Sun, J. Yao, J. Wang, H. Ming, A. Wang, and Q. Zhan, "Mode-locked all-fiber laser generating optical vortex pulses with tunable repetition rate," Appl. Phys. Lett. **112**, 261103 (2018).
22. J. Song, H. Xu, H. Wu, L. Huang, J. Xu, H. Zhang, and P. Zhou, "High power narrow linewidth LP_{11} mode fiber laser using mode-selective FBGs," Laser Phys. Lett. **15**, 115101 (2018).
23. D. Mao, T. Feng, W. Zhang, H. Lu, Y. Jiang, P. Li, B. Jiang, Z. Sun, and J. Zhao, "Ultrafast all-fiber based cylindrical-vector beam laser," Appl. Phys. Lett. **110**, 021107 (2017).
24. J. Zheng, A. Yang, T. Wang, N. Cao, M. Liu, F. Pang, T. Wang, and X. Zeng, "Switchable wavelength vortex beams based on polarization-dependent micro-knot resonator," Photon. Res. **6**, 396–402 (2018).
25. Z. Zhang, Y. Cai, J. Wang, H. Wan, and L. Zhang, "Switchable dual-wavelength cylindrical vector beam generation from a passively mode-locked fiber laser based on carbon nanotubes," IEEE J. Sel. Top. Quantum Electron. **24**, 1100906 (2018).
26. S. Yao, G. Ren, Y. Yang, Y. Shen, Y. Jiang, S. Xiao, and S. Jian, "Few-mode fiber Bragg grating-based multi-wavelength fiber laser with tunable orbital angular momentum beam output," Laser Phys. Lett. **15**, 095001 (2018).
27. L. G. Wright, D. N. Christodoulides, and F. W. Wise, "Spatiotemporal mode-locking in multimode fiber lasers," Science **358**, 94–97 (2017).
28. T. Wang, F. Shi, Y. Huang, J. Wen, Z. Luo, F. Pang, T. Wang, and X. Zeng, "High-order mode direct oscillation of few-mode fiber laser for high-quality cylindrical vector beams," Opt. Express **26**, 11850–11858 (2018).
29. H. Qin, X. Xiao, P. Wang, and C. Yang, "Observation of soliton molecules in a spatiotemporal mode-locked multimode fiber laser," Opt. Lett. **43**, 1982–1985 (2018).
30. G. D'Aguanno and C. R. Menyuk, "Nonlinear mode coupling in whispering-gallery-mode resonators," Phys. Rev. A **93**, 043820 (2016).
31. M. N. Zervas and C. A. Codemard, "High power fiber lasers: a review," IEEE J. Sel. Top. Quantum Electron. **20**, 219–241 (2014).
32. Y. Jiang, G. Ren, Y. Lian, B. Zhu, W. Jin, and S. Jian, "Tunable orbital angular momentum generation in optical fibers," Opt. Lett. **41**, 3535–3538 (2016).
33. Y. Shen, G. Ren, Y. Yang, S. Yao, S. Xiao, Y. Jiang, Y. Xu, Y. Wu, W. Jin, and S. Jian, "Generation of the tunable second-order optical vortex beams in narrow linewidth fiber laser," IEEE Photon. Technol. Lett. **29**, 1659–1662 (2017).
34. J. Liu, Y. Chen, Y. Li, H. Zhang, S. Zheng, and S. Xu, "Switchable dual-wavelength *Q*-switched fiber laser using multilayer black phosphorus as a saturable absorber," Photon. Res. **6**, 198–203 (2018).
35. F. Takahashi, K. Miyamoto, H. Hidai, K. Yamane, R. Morita, and T. Omatsu, "Picosecond optical vortex pulse illumination forms a monocrystalline silicon needle," Sci. Rep. **6**, 21738 (2016).
36. J. Wen, X. He, J. Xing, J. Yang, F. Pang, X. Zeng, Z. Chen, and T. Wang, "All-fiber OAM amplifier with high purity and broadband spectrum gain based on fused taper vortex-beam coupler," IEEE Photon. J. **10**, 7105308 (2018).
37. S. Li, Q. Mo, X. Hu, C. Du, and J. Wang, "Controllable all-fiber orbital angular momentum mode converter," Opt. Lett. **40**, 4376–4379 (2015).

38. R. Ismaeel, T. Lee, B. Oduro, Y. Jung, and G. Brambilla, "All-fiber fused directional coupler for highly efficient spatial mode conversion," Opt. Express **22**, 11610–11619 (2014).
39. Z. Luo, J. Liu, H. Wang, A. Luo, and W. Xu, "Wide-band tunable passively *Q*-switched all-fiber ring laser based on nonlinear polarization rotation technique," Laser Phys. **22**, 203–206 (2012).
40. M. Chernysheva, A. Bednyakova, M. Al Araimi, R. C. Howe, G. Hu, T. Hasan, A. Gambetta, G. Galzerano, M. Rümmeli, and A. Rozhin, "Double-wall carbon nanotube hybrid mode-locker in Tm-doped fibre laser: a novel mechanism for robust bound-state solitons generation," Sci. Rep. **7**, 44314 (2017).
41. Y. Zhao, Y. Liu, L. Zhang, C. Zhang, J. Wen, and T. Wang, "Mode converter based on the long-period fiber gratings written in the two-mode fiber," Opt. Express **24**, 6186–6195 (2016).
42. D. Lin, N. Baktash, M. Berendt, M. Beresna, P. Kazansky, W. Clarkson, S. Alam, and D. Richardson, "Radially and azimuthally polarized nanosecond Yb-doped fiber MOPA system incorporating temporal shaping," Opt. Lett. **42**, 1740–1743 (2017).